

# Aberrations in Temporal Imaging

Corey V. Bennett, *Student Member, IEEE*, and Brian H. Kolner, *Member, IEEE*

**Abstract**—Recent advances in temporal imaging allow construction of systems that can expand or compress arbitrary waveforms in time, while maintaining the shape of their envelope profile with subpicosecond resolution. The process is analogous to imaging in space, with the quadratic spectral phase introduced by narrow-band dispersion performing the time-domain role of paraxial diffraction and quadratic temporal phase modulation acting as a time lens. Higher order phase terms in the dispersive networks and the time lens modulation introduce aberrations into the system. The effect each aberration has on the final temporal image varies depending on the system configuration and where the source is located in the system. A theoretical and experimental study of aberration effects is presented in this article.

**Index Terms**—Dispersive propagation, frequency mixing, phase modulation, temporal imaging, time lens, ultrafast measurement, ultrafast pulse propagation.

## I. INTRODUCTION

THE GENERATION and characterization of ultrafast optical waveforms having long and complex structure is of growing importance. For example, experiments planned for the National Ignition Facility will require recording approximately 1 ns of a single-transient signal with subpicosecond, preferably 100 fs, resolution. While many measurement techniques with ultrafast resolution have been demonstrated, most require sampling of a repetitive signal and some are limited in the complexity (time-bandwidth product) of the signal that can be recorded [1]–[4]. Temporal imaging<sup>1</sup> [5]–[12] allows an arbitrarily shaped ultrafast waveform to be magnified or compressed in time while maintaining the shape of its envelope profile, thereby improving the resolution of an existing measurement system. It operates on a single-shot basis, generating a scaled replica of a waveform within the temporal field of view for each occurrence of time lens modulation [13].

Temporal imaging is based on a space–time analogy between paraxial diffraction and narrowband dispersion [14]–[18]. Both introduce quadratic phase filtering in their respective frequency domains;  $\phi \propto (k_x^2 + k_y^2)$  in space and  $\phi \propto \omega^2$  in

time. There is also a one-to-one analogy between the quadratic phase modulation performed in  $(x, y)$  by an ideal spatial lens and a quadratic phase modulation imparted in the local time coordinate  $\tau$  traveling with the imaged waveform. The device performing this operation is therefore considered a “time lens.” A temporal imaging system is constructed by cascading input dispersion, time lens modulation, and output dispersion, in the appropriate balance, analogous to the arrangement in a spatial imaging system. Each component can introduce aberrations because of departures from ideal quadratic phase. For example, the phase response of dispersive networks can generally be described by a Taylor series expansion. The second-order term is responsible for imaging properties, while third and higher order terms cause distortion. Similarly, an ideal time lens provides quadratic phase modulation and the presence of any higher order terms will degrade the temporal image. This paper analyzes the effects of deviations from ideal phase behavior in the dispersive networks and the time lens. These effects were considered in the design of the system presented in [19] and [20], although not discussed, and will be critical in future high-speed instrumentation based on temporal imaging. We also show that strategic combinations of different aberration sources can minimize the overall waveform distortion for a given application.

It is important to distinguish a few fundamental physical differences between components in spatial and temporal imaging systems. A space lens is generally made from a combination of curved surfaces between materials of different refractive indexes. The transverse phase it imparts depends on the curvature of these surfaces and the indexes of refraction on either side of the lens. We cannot precisely define the imparted phase without knowing the index of the medium surrounding the lens. We also have little control over the way a beam diffracts as it propagates in a homogeneous spatial system. For large ray angles we cannot simply alter the propagation characteristics to realize paraxial conditions. Clever choices of lens materials, curvatures, and positioning can all be combined to minimize the total system aberrations, but it is the system as a whole that must be engineered. In contrast, the active phase modulation of a time lens is independent of the dispersive networks before and after the lens. Therefore, the performance of each part of the imaging system may be optimized independently once a thorough understanding of the sources and effects of aberrations is in hand. We begin with dispersion.

## II. HIGHER ORDER PHASE EFFECTS IN DISPERSION

The wave equation for media with frequency-dependent permittivity  $\epsilon(\omega)$  may be solved by Fourier transformation to

Manuscript received July 24, 2000; revised September 27, 2000. This work was supported in part by the U.S. Department of Energy’s Lawrence Livermore National Laboratory under Contract W-7405-Eng-48, by the LLNL Photonics Group under Laboratory Directed Research and Development Grant 98-ERD-027, by the National Science Foundation, and by the David and Lucile Packard Foundation.

C. V. Bennett is with the Electrical Engineering Department, University of California, Los Angeles, CA 90032 USA and the Electronics Engineering Division, Lawrence Livermore National Laboratory, Livermore, CA 94551 USA.

B. H. Kolner is with the Department of Applied Science, University of California, Davis, CA 95616 USA.

Publisher Item Identifier S 0018-9197(01)00395-5.

<sup>1</sup>(See also U.S. Patent 3 283 080, Nov. 1966, and U.S. Patent 3 354 456, Nov. 1967.)

the frequency domain where convolution with the dielectric response becomes multiplication with the field spectrum

$$\frac{\partial^2 \mathcal{E}(z, \omega)}{\partial z^2} = -\omega^2 \mu \epsilon(\omega) \mathcal{E}(z, \omega) = -\beta^2(\omega) \mathcal{E}(z, \omega). \quad (1)$$

For unidirectional wave motion the solution is

$$\mathcal{E}(z, \omega) = \mathcal{E}(0, \omega) \exp[-i\beta(\omega)z]. \quad (2)$$

Now, we are interested in the effects of higher-order phase terms on the propagation of an envelope waveform  $A(z, t)$  associated with the electric field

$$E(z, t) = A(z, t) \exp[i(\omega_0 t - \beta_0 z)] \quad (3)$$

where  $\beta_0$  is the propagation constant at the carrier frequency  $\omega_0$ . The Fourier spectrum of this waveform is

$$\mathcal{E}(z, \omega) = \mathcal{A}(z, \omega - \omega_0) \exp(-i\beta_0 z) \quad (4)$$

where  $\mathcal{A}(z, \omega - \omega_0)$  is the baseband spectrum of the envelope  $A(z, t)$  translated to the carrier. There is a distinct difference between (2) and (4). Equation (2) describes the effects of propagation on an initial spectrum while (4) is merely a statement of the spectrum of a specific waveform (3). How it evolved upon propagation is not revealed. However, if it is to satisfy the wave equation, it must obey the propagation law (2) and therefore, by equating the two, we find

$$\mathcal{A}(z, \omega - \omega_0) = \mathcal{A}(0, \omega - \omega_0) \exp(-i[\beta(\omega) - \beta_0]z) \quad (5)$$

where  $\mathcal{A}(0, \omega - \omega_0) \equiv \mathcal{E}(0, \omega)$ . Now it is straightforward to include the effects of the frequency dependence of  $\beta(\omega)$  by, for example, expanding it in a Taylor series about the carrier to the desired order of accuracy

$$\begin{aligned} \beta(\omega) = & \beta_0 + (\omega - \omega_0)\beta' + (\omega - \omega_0)^2 \frac{\beta''}{2!} \\ & + (\omega - \omega_0)^3 \frac{\beta'''}{3!} + \dots + (\omega - \omega_0)^n \frac{\beta^{(n)}}{n!}. \end{aligned} \quad (6)$$

Thus, the envelope spectrum propagates according to

$$\mathcal{A}(z, \Omega) = \mathcal{A}(0, \Omega) \exp\left[-i\left(\Omega\beta' + \Omega^2 \frac{\beta''}{2!} + \dots\right)z\right] \quad (7)$$

where  $\Omega \equiv \omega - \omega_0$  is a baseband spectral component. The total dispersed electric field is found by inverse Fourier transformation;  $\mathcal{F}^{-1}\{\mathcal{A}(z, \Omega)\} = A(z, t)$  and substitution into (3).

The problem can be further simplified by converting to the traveling-wave reference frame  $\tau = t - \beta'z$  and  $\xi = z$ . This transformation effectively drops the first-order group delay term  $\xi\beta'$ , resulting in

$$\mathcal{A}(\xi, \Omega) = \mathcal{A}(0, \Omega) \exp\left[-i\left(\Omega^2 \frac{\xi\beta''}{2!} + \Omega^3 \frac{\xi\beta'''}{3!} + \dots\right)\right]. \quad (8)$$

Thus, in a traveling-wave coordinate system, the distortion of an envelope function is determined by the effects of the higher order terms in the expansion of  $\beta(\omega)$  upon the spectrum of the envelope.

Since dispersion characteristics often change for different regions of a dispersive system it is often easier to work with the total spectral phase  $\phi(\omega) = \sum_n \xi_n \beta_n(\omega)$ . Thus  $\phi'$  is a total

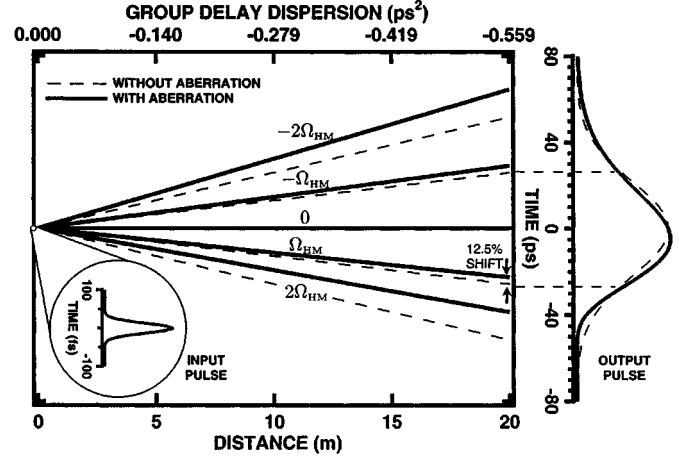


Fig. 1. A calculated temporal ray diagram showing dispersive propagation. The horizontal axis is the distance or accumulated GDD  $\phi''$  through which the signal has propagated. The vertical axis is the local time  $\tau$ . Dashed lines show the ideal paths of various spectral components while solid lines represent the actual paths in the presence of third-order dispersive aberration.  $\beta'''/\beta''$  is that of fused silica at  $\lambda = 1550$  nm.

group delay and  $\phi''$  is a total group delay dispersion (GDD), each evaluated at the carrier frequency. The GDD  $\phi''$  in (8) imparts the desired quadratic spectral phase while higher order terms introduce aberration.

A useful method for visualizing the propagation of a signal utilizes the concept of a time ray [21], [22], the relative space-time path of a particular spectral component in a traveling-wave coordinate system (Fig. 1). Each ray is associated with a spectral component  $\Omega$  and has a trajectory given by its deviation from the traveling-wave origin  $\tau = 0$  as a function of the normalized propagation distance  $\xi\beta'' = \phi''$ . This can be seen by calculating the group delay experienced at other frequencies near the carrier

$$\begin{aligned} t_g(\omega) &= \frac{z}{v_g(\omega)} = z \frac{d\beta(\omega)}{d\omega} \\ &= z \left( \beta' + (\omega - \omega_0)\beta'' + (\omega - \omega_0)^2 \frac{\beta'''}{2!} + \dots \right). \end{aligned} \quad (9)$$

The group delay of a particular baseband envelope spectral component  $\Omega = \omega - \omega_0$ , relative to the traveling-wave coordinate system moving with the optical signal, is

$$\begin{aligned} \tau_g(\Omega) &= t_g(\omega) - t_g(\omega_0) \\ &= \Omega\xi\beta'' + \Omega^2 \frac{\xi\beta'''}{2!} + \Omega^3 \frac{\xi\beta''''}{3!} + \dots \\ &= \Omega\phi'' + \Omega^2 \frac{\phi'''}{2!} + \Omega^3 \frac{\phi''''}{3!} + \dots. \end{aligned} \quad (10)$$

A given spectral component entering a dispersive delay line at an initial time  $\tau_{in}$  experiences a frequency-dependent delay and leaves at  $\tau_{out}(\Omega) = \tau_{in} + \tau_g(\Omega)$ . The space-time slope  $d\tau(\Omega)/d\phi'' = d\tau_g(\Omega)/d\phi''$  is simply the frequency  $\Omega$  plus distortions that result from higher order dispersion terms

$$\frac{d\tau(\Omega)}{d\phi''} = \Omega \left[ 1 + \frac{\Omega}{2!} \frac{\beta'''}{\beta''} + \frac{\Omega^2}{3!} \frac{\beta''''}{\beta''} + \dots + \frac{\Omega^{n-2}}{(n-1)!} \frac{\beta^{(n)}}{\beta''} \right]. \quad (11)$$

These dispersive aberrations can be ignored if

$$\frac{\Omega}{2!} \frac{\beta'''}{\beta''}, \frac{\Omega^2}{3!} \frac{\beta''''}{\beta''}, \dots, \frac{\Omega^{n-2}}{(n-1)!} \frac{\beta^{(n)}}{\beta''} \ll 1 \quad (12)$$

over the frequency range of interest  $\Delta\omega$ , as determined by the bandwidth of the signal or any spectral filtering processes in the system [23]. We will use the half-maximum frequency  $\Omega_{\text{HM}} \equiv \Delta\omega/2$  to evaluate the relative importance of these aberrations.

Fig. 1 is a temporal ray diagram showing the dispersion of a 30-fs pulse. The dashed lines show ideal paths with slopes corresponding to their frequency  $\Omega$  while the solid lines include the distortion that results from the third-order dispersive aberration in (11). While the ray approach does not give a complete solution to the envelope, it is an intuitive tool for visualizing the effects of aberrations. The actual output envelope in Fig. 1 was calculated using (8) and is consistent with the ray modeling approach. In this example,  $(\Omega_{\text{HM}}\beta''')/(2!\beta'') = -0.125$  and we see that the  $\pm\Omega_{\text{HM}}$  frequencies have shifted 12.5% from their delay in an ideal system. Higher frequency components are shifted even more and the superposition of all components produces a pulse that is distorted to one side. As the magnitude of  $\beta'''$  increases further (Fig. 2), different spectral components within the signal bandwidth start having the same group delay, the span of time rays is strongly distorted to one side, and the interference of these spectral components produces a long tail of decaying oscillations [24]. The important equations, (8) and (10), for both modeling approaches are gathered in Table I.

It should be noted that  $\omega_0$  in this analysis represents a general carrier frequency. In systems using a parametric time lens, the carrier will change due to the frequency conversion process. Each dispersive delay line must then be evaluated at this new frequency.

### III. HIGHER ORDER PHASE EFFECTS IN TIME LENS MODULATION

The function of an ideal time lens is to impart a quadratic *temporal* phase, or equivalently, an instantaneous frequency chirp  $d\omega_i/d\tau = d^2\Phi(\tau)/d\tau^2|_{\tau=0}$ , where  $\Phi(\tau)$  is the imparted time lens phase profile. The ideal envelope out of the time lens is  $A_{\text{out}}(\tau) = A_{\text{in}}(\tau)H(\tau)P(\tau)$ , where

$$H(\tau) = \exp(i\Phi(\tau)) = \exp\left(\frac{-i\tau^2}{2\phi_f''}\right) \quad (13)$$

is the time lens phase modulation function and  $P(\tau)$  is the amplitude modulation, or pupil, function. For simplicity, we will ignore many of the finite temporal aperture effects which are discussed in more detail elsewhere [10], [11], [23]. The modulation strength is characterized by a physical focal length  $\xi_f$  or a focal GDD

$$\phi_f'' \equiv \xi_f\beta'' \equiv -(d\omega_i/d\tau)^{-1} \quad (14)$$

which can be shown to be the dispersion required to remove the frequency chirp that has just been imparted.

Early optical time lenses were produced using electro-optic phase modulators [25]–[32]. An electrooptic time lens

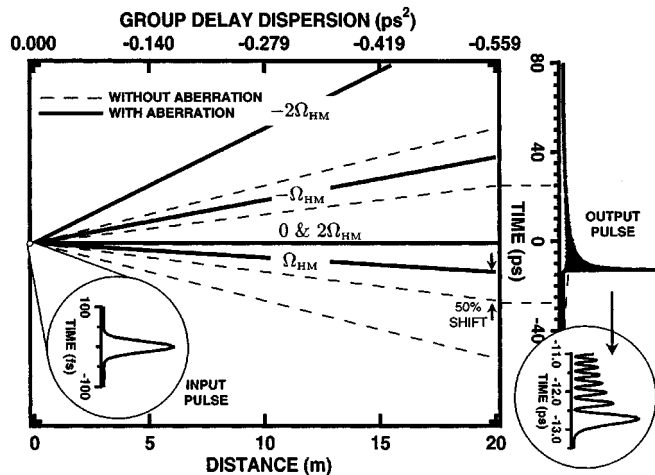


Fig. 2. A calculated temporal ray diagram showing strong dispersive aberration. Dashed lines show the ideal spectral paths while solid lines represent the actual paths in the presence of third-order spectral phase.  $\beta'''/\beta''$  is four times that of fused silica at  $\lambda = 1550$  nm.

driven at a modulation frequency  $\omega_m$  has a phase profile  $\Phi(\tau) \propto \cos(\omega_m\tau)$ , which is only approximately quadratic at a cusp of the sinusoid. Care has to be taken to restrict the signal to a usable aperture  $\tau_a \approx 1/\omega_m$  centered on a cusp or higher order phase terms will produce aberrations in the system [10], [29]. Other time lens mechanisms have also been demonstrated. In the case of cross-phase modulation [33], the imparted phase profile is determined by the pump pulse intensity profile.

The resolution of the imaging system in the absence of any aberrations is inversely proportional to the bandwidth imparted by the modulation process;  $\delta\tau \propto 1/\Delta\omega$ . Fundamental technical challenges in obtaining a strong quadratic phase modulation over a long temporal window with minimum higher-order phase limits the bandwidth and thus the performance of those approaches.

On the other hand, linearly frequency-swept optical pulses with very large bandwidths are easily produced with various other techniques, such as dispersing pulses from femtosecond lasers. Combining these pump pulses with the dispersed signal waveform by nonlinear mixing imparts the quadratic phase of the pump to the signal at the sum or difference frequency and therefore achieves the desired time lens action. Our recent work has concentrated on these parametric time lenses and their applications to temporal imaging [19],[20],[34]. Numerous idealized configurations using both sum- and difference-frequency generation (SFG and DFG) have been analyzed [21]. In a companion paper we investigated limitations to the resolution and field of view that result from spectral filtering effects in these systems [23]. An additional benefit of this technique is that the phase profile of the pump pulse can be adjusted through carefully controlled dispersive propagation or Fourier transform pulse shaping [35], [36]. In principle, an exactly quadratic temporal phase can be imparted with this technique, producing an ideal time lens phase profile.

A realistic time lens phase profile may be described by the series expansion

$$\Phi(\tau) = \Phi_0 + \tau\Phi' + \tau^2\frac{\Phi''}{2!} + \tau^3\frac{\Phi'''}{3!} + \dots + \tau^n\frac{\Phi^{(n)}}{n!} \quad (15)$$

TABLE I  
EQUATIONS MODELING THE COMPONENTS OF A TEMPORAL IMAGING SYSTEM. THE TERMS IN SQUARE BRACKETS  
ARE RESPONSIBLE FOR ABERRATIONS IN THE SYSTEM

System element	Modeling approach	Equations
Dispersion	Ray	$\tau_{\text{out}} = \tau_{\text{in}} + \Omega \phi'' + \left[ \Omega^2 \frac{\phi'''}{2!} + \Omega^3 \frac{\phi''''}{3!} + \dots \right], \quad \Omega_{\text{out}} = \Omega_{\text{in}}$
	Envelope	$\mathcal{A}_{\text{out}}(\Omega) = \mathcal{A}_{\text{in}}(\Omega) \exp\left(-i \left( \Omega^2 \frac{\phi'''}{2!} + \left[ \Omega^3 \frac{\phi'''}{3!} + \Omega^4 \frac{\phi''''}{4!} + \dots \right] \right)\right)$
Time Lens	Ray	$\tau_{\text{out}} = \tau_{\text{in}}, \quad \Omega_{\text{out}} = \Omega_{\text{in}} + \tau \Phi'' + \left[ \tau^2 \frac{\Phi'''}{2!} + \tau^3 \frac{\Phi''''}{3!} + \dots \right]$
	Envelope	$A_{\text{out}}(\tau) = A_{\text{in}}(\tau) \exp\left(i \left( \tau^2 \frac{\Phi'''}{2!} + \left[ \tau^3 \frac{\Phi'''}{3!} + \tau^4 \frac{\Phi''''}{4!} + \dots \right] \right)\right)$

where  $\Phi_0$  is a constant which may be ignored. Each derivative is with respect to time and evaluated at the center of the time lens  $\tau = 0$ . The instantaneous frequency imparted by the lens is given by the derivative of the phase  $\omega_i(\tau) = d\Phi(\tau)/d\tau$  and, of course, this spectrum is added to (or subtracted from) that of the input waveform. The constant term,  $\omega_i(0) = \Phi'$ , is a frequency offset from the input carrier which, if stable, plays no important role in the image formation. It may result from the SFG or DFG mixing in the parametric time lens or an imperfect quadratic phase in an electro-optic time lens. In either case, we may drop this static term and define the instantaneous frequency shift due to the time lens as

$$\begin{aligned} \Omega_L(\tau) &\equiv \frac{d\Phi(\tau)}{d\tau} - \left[ \frac{d\Phi(\tau)}{d\tau} \right]_{\tau=0} \\ &= \tau \Phi'' \left( 1 + \frac{\tau \Phi'''}{2! \Phi''} + \dots + \frac{\tau^{n-2}}{(n-1)!} \frac{\Phi^{(n)}}{\Phi''} \right). \end{aligned} \quad (16)$$

A time ray representing a frequency  $\Omega_{\text{in}}$  entering a conventional time lens at a time  $\tau$  will be frequency shifted to  $\Omega_{\text{out}} = \Omega_{\text{in}} + \Omega_L(\tau)$ . This ‘‘bends’’ the time ray since it must propagate through the output dispersion in accordance with (11). By dropping the static frequency offset from our definition of  $\Omega_L(\tau)$ , we have ‘‘aligned’’ the output dispersive network with whatever new carrier frequency is generated. The temporal ray perspective is again a powerful technique for understanding the underlying physical process that is occurring in the time lens.

The third and higher order temporal phase terms in (16) have made the imparted frequency chirp time-dependent,  $d\omega_i(\tau)/d\tau = d\Omega_L(\tau)/d\tau$ , producing a time-dependent focal GDD

$$\begin{aligned} \frac{-1}{\phi_f''(\tau)} &= \frac{d\Omega_L(\tau)}{d\tau} \\ &= \Phi'' \left( 1 + \tau \frac{\Phi'''}{\Phi''} + \frac{\tau^2}{2!} \frac{\Phi''''}{\Phi''} + \dots \right). \end{aligned} \quad (17)$$

The chirp rate imparted at the center of the lens is simply  $\Phi''$ , thus the central focal GDD is  $\phi_f''(0) = -1/\Phi''$ . Higher order terms produce a distortion that increases as  $|\tau_{\text{in}}|$  increases and we get closer to the edges of the time lens aperture  $P(\tau)$ . We may ignore the higher order terms if the frequency perturbation they produce in (16) is small

$$\frac{\tau}{2!} \frac{\Phi'''}{\Phi''}, \frac{\tau^2}{3!} \frac{\Phi''''}{\Phi''}, \dots, \frac{\tau^{n-2}}{(n-1)!} \frac{\Phi^{(n)}}{\Phi''} \ll 1 \quad (18)$$

over the width of  $P(\tau)$ , but this may not always be the case. Like  $\Omega_{\text{HM}}$ , the half-maximum transmission point,  $\tau_{\text{HM}} = \tau_a/2$ , where  $\tau_a$  is the full width at half maximum of  $P(\tau)$ , is a convenient time at which to note the strength of these aberrations.

Fig. 3 shows how a third-order time lens phase aberration would manifest itself in a pulse compression application. The input can be viewed as a very long, narrow bandwidth pulse or simply continuous wave light. The lens has phase terms  $\Phi'' = 2\pi \times 285 \text{ GHz/ps}$  and  $\Phi''' = 2\pi \times 2.76 \text{ GHz/ps}^2$ , and a Gaussian pupil function with  $\tau_a = 51.6 \text{ ps}$ . The output of the time lens has a very broad bandwidth, which, if imparted only linearly, would result in a compressed 30-fs pulse one focal dispersion  $\phi_f''$  from the time lens. Instead, the aberration produces a nonlinear frequency shift, which in this example gives  $(\tau_{\text{HM}} \Phi''')/(2! \Phi'') = -0.125$ , and results in a 12.5% error in the imparted frequency (16) and thus the delay through the output dispersion  $\Omega_{\text{out}} \phi_f''$ , for a time ray entering the lens at  $\tau_{\text{HM}}$ . Third-order temporal phase causes a frequency shift and output time delay that are shifted to one side, producing a blurred tail analogous to coma in spatial systems. A fourth-order term would cause a frequency shift, or focal dispersion change, that is symmetric about  $\tau = 0$ . This is analogous to how the focal length varies symmetrically about the optical axis in the common case of spherical aberration for spatial lenses.

Again, the time ray approach is a useful tool to visualize the space-time flow of energy in the traveling-wave coordinate system, but since it does not quantify amplitude or interference effects it does not reproduce the actual output waveform. We can visualize amplitude effects by shading the lens to represent  $P(\tau)$  and varying ray line thicknesses to represent their relative spectral intensities, as shown in Fig. 3. The total effect of the time lens may be modeled by utilizing the full envelope expressions or we can derive physically insightful expressions that indicate approximate system results by tracking the path of individual rays. The expressions for both approaches are again collected in Table I.

It should be noted that the complex conjugate produced by a DFG time lens [21] can introduce sign changes in many of the equations in this article. Aberration effects in conventional time lens systems still apply to DFG systems, although in some configurations the results may have to be spectrally or temporally reversed. This distinction will be ignored in the remainder of this paper.

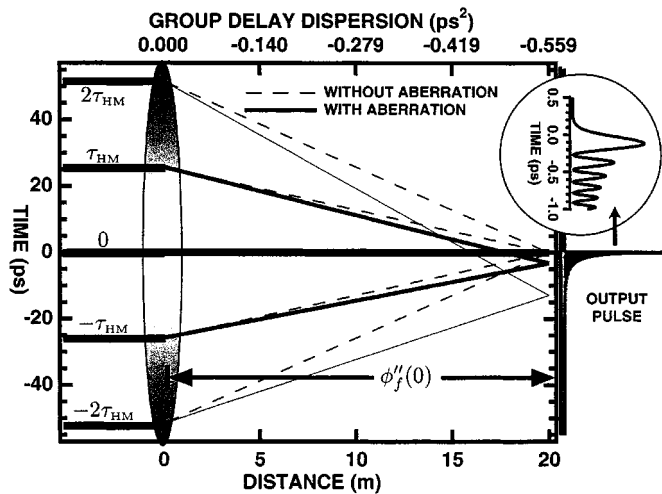


Fig. 3. A calculated pulse compression ray diagram with aberration caused by third-order time lens phase. Nonlinearity in the imparted frequency chirp makes the focal dispersion  $\phi_f''$  dependent on the input time. Ray thickness indicates intensity due to Gaussian pupil function.

#### IV. TEMPORAL IMAGING

##### A. Ideal Temporal Imaging

In an ideal system, propagating an input waveform  $A_{in}(\tau)$  through an input GDD  $\phi_1''$ , a time lens modulation characterized by a focal GDD  $\phi_f''$ , and an output GDD  $\phi_2''$ , in accordance with the temporal imaging condition

$$\frac{1}{\phi_1''} + \frac{1}{\phi_2''} = \frac{1}{\phi_f''} \quad (19)$$

produces an output waveform [10]

$$A_{out}(\tau) = \frac{1}{\sqrt{M}} \exp\left(\frac{-i\tau^2}{2M\phi_f''}\right) A_{in}(\tau/M) \quad (20)$$

where the temporal magnification is given by

$$M = -\frac{\phi_2''}{\phi_1''} = 1 - \frac{\phi_2''}{\phi_f''} = \left(1 - \frac{\phi_1''}{\phi_f''}\right)^{-1}. \quad (21)$$

The last two forms of the magnification are convenient when propagating time rays through focused systems, such as those discussed in Section V. The output is a temporally scaled replica of the input waveform with a residual frequency chirp equal to that which is imparted by the time lens divided by the system magnification.

##### B. LaGrange Invariant

A very useful quantity in spatial geometric optics is the LaGrange invariant [37]–[39], an expression relating the slope and position of any two rays that is constant everywhere in an ideal system. Once determined it can be used to find ray parameters at other places in the system, skipping many of the intermediate steps. It also provides a standard from which to measure the effects of aberrations.

Consider the propagation of two rays through an ideal temporal imaging system as shown in Fig. 4. To find a time domain

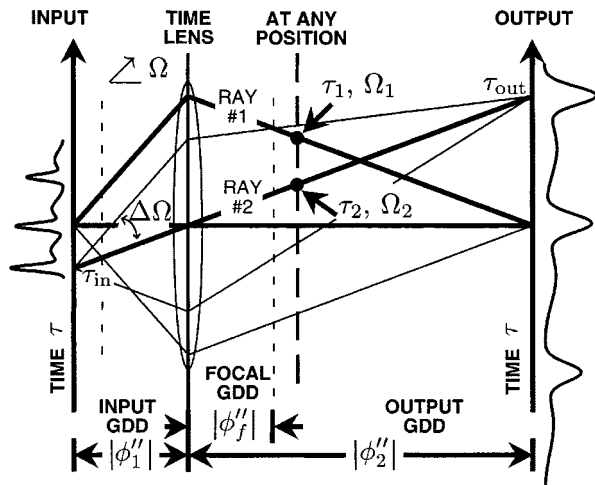


Fig. 4. Ray diagram schematic of an ideal temporal imaging system. For any two time rays, there is a relationship between their arrival times and frequencies that is constant everywhere in an ideal system, the temporal LaGrange invariant (25).

equivalent of the LaGrange invariant, we must find a quantity relating these two time rays that remains constant with dispersive propagation (in the narrowband approximation) and that is also unchanged by the linear frequency chirp imparted by the ideal time lens.

Neglecting the higher order terms in (10), through any section of ideal dispersive propagation the two rays must satisfy

$$\tau_{1,out} = \tau_{1,in} + \Omega_1 \phi'' \quad \text{and} \quad \tau_{2,out} = \tau_{2,in} + \Omega_2 \phi''. \quad (22)$$

Relating these two rays through the common GDD

$$\frac{\tau_{1,out} - \tau_{1,in}}{\Omega_1} = \phi'' = \frac{\tau_{2,out} - \tau_{2,in}}{\Omega_2}. \quad (23)$$

Collecting terms from the input on the left and the output on the right gives

$$\tau_{1,in}\Omega_2 - \tau_{2,in}\Omega_1 = \tau_{1,out}\Omega_2 - \tau_{2,out}\Omega_1. \quad (24)$$

Although these rays will move in time relative to the center of the wave packet, the difference in arrival time of one ray multiplied by the carrier frequency of the other is unchanged by the dispersive propagation. A similar process can be followed using (16) (neglecting higher order terms) to investigate the frequency change of these two rays upon propagation through an ideal lens. Relating the two expressions that result through the focal dispersion, we again find that the quantity

$$I = \tau_1\Omega_2 - \tau_2\Omega_1 \quad (25)$$

the temporal equivalent of the LaGrange invariant, is also unchanged by the modulation of an ideal lens and we must conclude that it is constant everywhere in an ideal temporal imaging system.

The rays shown in Fig. 4 are a special case that can be insightful. Ray #1, in particular, is an axial ray having an initial input time of  $\tau_{1,in} = 0$  at the object position and is imaged at

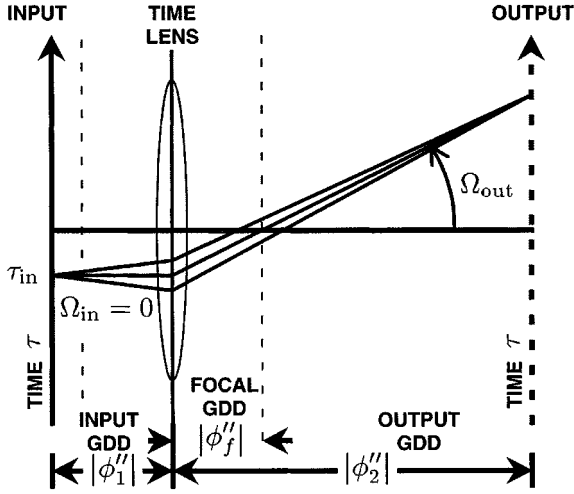


Fig. 5. Temporal ray diagram of the Spectrally Resolved Up-conversion technique [40]. Recording  $\Omega_{\text{out}}$  versus  $\tau_{\text{in}}$  gives a measure of the time lens chirp and thus its focal dispersion  $\phi'_f$ . This approach was also used to measure the input dispersion (see Section VI).

the output to  $\tau_{1,\text{out}} = 0$ . Ray #2 can be any oblique ray. Evaluating the temporal LaGrange invariant (25) at both the object and image positions gives

$$\tau_{2,\text{in}}\Omega_{1,\text{in}} = \tau_{2,\text{out}}\Omega_{1,\text{out}} \quad (26)$$

or

$$M = \frac{\tau_{2,\text{out}}}{\tau_{2,\text{in}}} = \frac{\Omega_{1,\text{in}}}{\Omega_{1,\text{out}}}. \quad (27)$$

We see that the magnification of the ideal system is not only given by the ratio of the arrival time at the image to the initial time at the object for any off-axis ( $\tau_{\text{in}} \neq 0$ ) ray but is also given by the reduction in frequency for the axial ray.

Other forms of the LaGrange invariant formulas are often used as a basis for measuring aberrations. When a ray enters a lens parallel to the lens axis, the exit angle depends on the displacement of the input ray from the axis. The output acquires a new spatial frequency corresponding to this exit angle. In spatial lens design, coma can be tested by plotting the ratio  $h_{\text{in}}/\sin\theta_{\text{out}}$  [39], where  $h_{\text{in}}$  is the offset of the incident ray, and  $\theta_{\text{out}}$  is the angle the output ray makes with the optical axis. To prevent coma, this value, which is equal to the focal distance measured along the image ray, must be constant for all heights of the input ray.

The time domain equivalent to this test can be performed by scanning a time lens with an input pulse which has a reduced bandwidth centered at  $\Omega = 0$ , as shown in Fig. 5. By definition, this input pulse would propagate “parallel” to the temporal optical axis, staying at a fixed offset time while propagating through the input dispersion. Scanning the input time  $\tau_{\text{in}}$  and measuring the output frequency  $\Omega_{\text{out}}$ , we should find that the quantity  $-\tau_{\text{in}}/\Omega_{\text{out}}$  is constant and equal to the focal GDD  $\phi''_f$ . Any deviation indicates higher order phase terms that produce aberrations in the system. Although not presented in the context of time rays or temporal imaging,

the measurement technique known as “Spectrally Resolved Up-conversion” [40] is essentially this process and was used to characterize both the time lens and input dispersion in our system (see Section VI).

### C. Misfocus in Ideal Temporal Imaging

Configuration errors or fluctuations in the temporal imaging system can misfocus it, producing a slightly blurred signal even in the absence of higher order phase aberrations. Time lens modulation is an active process, thus the focal dispersion may change due to instabilities in the modulation process, such as changes in the pump laser pulse of a parametric time lens. Dispersive systems may have a different GDD at slightly different wavelengths. If the center wavelength of the pump or input signal drifts, their effective GDD may change. Their GDD may also vary slightly due to thermal or mechanical instabilities. There is always some uncertainty in the accuracy with which system components are configured.

Consider a general time ray propagating through a temporal imaging system as described by the expressions in Table I. (Throughout the derivations that follow subscripts [in] and [out] will refer to values at the input and output of the system, while  $[L, \text{in}]$  and  $[L, \text{out}]$  will refer to the input and output of the time lens.) The input ray could be depicted by any one of the rays in the bundle around Ray #2 in Fig. 4, with its ideal path shown in the figure. If Ray #2 originates from  $\tau_{\text{in}}$ , it must have a frequency  $\Omega_{\text{in}} = -\tau_{\text{in}}/\phi'_1$  in order to propagate through the center of the lens. Any other ray in the bundle originating from  $\tau_{\text{in}}$  may have a frequency  $\Omega_{\text{in}} = (-\tau_{\text{in}}/\phi'_1) + \Delta\Omega$ , where  $\Delta\Omega$  is some frequency offset. Thus this ray is completely general in that its input time can be adjusted by choosing  $\tau_{\text{in}}$  and its input frequency  $\Omega_{\text{in}}$  is adjusted by choosing  $\Delta\Omega$ . We may propagate this ray through the temporal imaging system, allowing for a slight misfocus by simply not imposing the imaging condition (19) or magnification expressions (21).

At the input to the time lens, the ray time and frequency are  $\tau_{L,\text{in}} = \phi''_1\Delta\Omega$ , and  $\Omega_{L,\text{in}} = \Omega_{\text{in}}$ . The lens output time is unchanged,  $\tau_{L,\text{out}} = \tau_{L,\text{in}}$ , but it is frequency shifted to

$$\Omega_{L,\text{out}} = \Omega_{L,\text{in}} - \frac{\tau_{L,\text{in}}}{\phi''_f} = \frac{-\tau_{\text{in}}}{\phi'_1} + \left(1 - \frac{\phi''_1}{\phi''_f}\right)\Delta\Omega. \quad (28)$$

The first term is simply the unmodified frequency that propagates through the center of the time lens, such as that of Ray #2. The second term shows that the input frequency difference  $\Delta\Omega$  is modified. In a focused system the fractional difference between the input and focal dispersion is the reciprocal of the ideal magnification (21). For example, a magnification of  $M = +100$  requires  $(\phi''_1 - \phi''_f)/\phi''_f = -0.01$  which dramatically reduces the frequency offset. This is also expected from the LaGrange invariant (25), knowing that two rays originating from the same input time would ideally focus to the same output time. Since their ideal output time is magnified, their frequency difference must be reduced by the magnification.

The frequency of the system is unchanged from that exiting the lens,  $\Omega_{\text{out}} = \Omega_{L,\text{out}}$ , but the time of each ray will be

shifted by the output dispersion

$$\begin{aligned}
\tau_{\text{out}} &= \tau_{L,\text{out}} + \Omega_{L,\text{out}} \phi_2'' \\
&= \phi_1'' \Delta\Omega - \frac{\phi_2''}{\phi_1''} \tau_{\text{in}} + \left(1 - \frac{\phi_1''}{\phi_f''}\right) \Delta\Omega \phi_2'' \\
&= \frac{-\phi_2''}{\phi_1''} \tau_{\text{in}} + \phi_1'' \Delta\Omega \left[1 - \frac{-\phi_2''}{\phi_1''} \left(1 - \frac{\phi_1''}{\phi_f''}\right)\right] \quad (29) \\
&= \frac{-\phi_2''}{\phi_1''} \tau_{\text{in}} + \phi_1'' \phi_2'' \Delta\Omega \left[\frac{1}{\phi_1''} + \frac{1}{\phi_2''} - \frac{1}{\phi_f''}\right]. \quad (30)
\end{aligned}$$

Consider the response of this system to an impulse at  $\tau_{\text{in}}$ . The first term in (29) and (30) is the ideally magnified output time. The transmitted spectrum would be centered at  $\Omega_{\text{in}} = -\tau_{\text{in}}/\phi_1''$  and propagate along Ray #2. The arrival time of the impulse would be magnified by  $-\phi_2''/\phi_1''$  but other spectral components  $\Omega_{\text{in}} = -\tau_{\text{in}}/\phi_1'' + \Delta\Omega$  might not focus to the same output time, as determined by the error produced by the second term which blurs the impulse response. The square bracketed term in (29) contains two versions of the magnification (21), which if properly focused would cancel. Expressed in an alternate form, the bracketed term in (30) is recognized as an imaging condition (19) error.

It is important to recognize that small errors in the input or focal dispersion can produce significant blurring for systems with large magnification. Continuing the  $M = +100$  example from above, if  $\phi_1''$  and  $\phi_f''$  are known to  $\pm 25\%$  then the error in their percent difference could be  $\pm 50\%$  of the difference, i.e.,  $(\phi_1'' - \phi_f'')/\phi_f'' = -0.010 \pm 0.005$ . Knowing that  $\phi_1'' \approx \phi_f''$  and assuming the input bandwidth is approximately the same as the time lens modulation bandwidth,  $\phi_1'' \Delta\Omega$  for the larger spectral components is comparable to the time lens duration or the system's input field of view [18]. An additional blurring at the output on the order of half the time lens duration would be reasonable to expect. Fine tuning capability is crucial for getting such a system properly focused and the stability of the time lens modulation and input dispersion are very important for maintaining proper focus. The same is true for output and focal dispersion errors in systems with large compression  $|M| \ll 1$ .

## V. SPECTRAL AND TEMPORAL PHASE ABERRATIONS

To investigate the aberration effects of various higher order phase terms in an imaging system, we may calculate the ray aberration, both the spectral and temporal output errors, again utilizing the propagation equations summarized in Table I. Analyzing each type of aberration source independently, for various input ray conditions, will lead to a better understanding of the significant effects each produces.

Consider a general time ray entering a focused temporal imaging system, i.e., (19) is satisfied and thus (21) can be applied. We will again utilize a general input ray with a time  $\tau_{\text{in}}$  and a frequency  $\Omega_{\text{in}} = (-\tau_{\text{in}}/\phi_1'') + \Delta\Omega$ , depicted by one of the rays in the bundle around Ray #2 in Fig. 4. Throughout the remainder of this article, the perturbation from ideal time ray propagation shown in the figure will be kept in square brackets.

### A. Output Dispersive Aberrations

Assuming an ideal input dispersion and time lens modulation, the output time from the lens and frequency from the system are unchanged from those in Section IV.C, except that now the magnification (21) may be used to simplify the expressions. That is  $\tau_{L,\text{out}} = \phi_1'' \Delta\Omega$  and

$$\Omega_{\text{out}} = \Omega_{L,\text{out}} = \frac{-\tau_{\text{in}}}{\phi_1''} + \frac{\Delta\Omega}{M}. \quad (31)$$

The time of each ray will be distorted by the output dispersive aberrations

$$\begin{aligned}
\tau_{\text{out}} &= \tau_{L,\text{out}} + \Omega_{L,\text{out}} \phi_2'' \\
&+ \left[ \Omega_{L,\text{out}}^2 \frac{\phi_2''}{2!} + \Omega_{L,\text{out}}^3 \frac{\phi_2''}{3!} + \dots \right] \\
&= M\tau_{\text{in}} + \left[ \Omega_{L,\text{out}}^2 \frac{\phi_2''}{2!} + \Omega_{L,\text{out}}^3 \frac{\phi_2''}{3!} + \dots \right]. \quad (32)
\end{aligned}$$

Thus, the output temporal error depends on the output frequency (31), which is unaffected by this aberration, but which is modified by the time lens.

### B. Input Dispersive Aberrations

At the input to the time lens the frequency is unchanged, i.e.,  $\Omega_{L,\text{in}} = \Omega_{\text{in}}$ . The arrival time at the lens, including the input dispersive aberration, becomes

$$\begin{aligned}
\tau_{L,\text{in}} &= \tau_{\text{in}} + \Omega_{\text{in}} \phi_1'' + \left[ \Omega_{\text{in}}^2 \frac{\phi_1''}{2!} + \Omega_{\text{in}}^3 \frac{\phi_1''}{3!} + \dots \right] \\
&= \Delta\Omega \phi_1'' + \left[ \Omega_{\text{in}}^2 \frac{\phi_1''}{2!} + \Omega_{\text{in}}^3 \frac{\phi_1''}{3!} + \dots \right]. \quad (33)
\end{aligned}$$

After an ideal time lens, the time of the ray is unchanged,  $\tau_{L,\text{out}} = \tau_{L,\text{in}}$ , but its frequency is shifted

$$\begin{aligned}
\Omega_{\text{out}} &= \Omega_{L,\text{out}} = \Omega_{L,\text{in}} - \frac{\tau_{L,\text{in}}}{\phi_f''} \\
&= \frac{-\tau_{\text{in}}}{\phi_1''} + \frac{\Delta\Omega}{M} - \left[ \frac{1}{\phi_f''} \left( \Omega_{\text{in}}^2 \frac{\phi_1''}{2!} + \Omega_{\text{in}}^3 \frac{\phi_1''}{3!} + \dots \right) \right]. \quad (34)
\end{aligned}$$

The first two terms represent the ideal frequency out of the time lens (31). The term in the square brackets is a perturbation in the output frequency that results from the input dispersive temporal error in (33).

After propagating through ideal output dispersion the ray is shifted to a time

$$\begin{aligned}
\tau_{\text{out}} &= \tau_{L,\text{out}} + \Omega_{L,\text{out}} \phi_2'' \\
&= \Delta\Omega \phi_1'' + \left[ \Omega_{\text{in}}^2 \frac{\phi_1''}{2!} + \Omega_{\text{in}}^3 \frac{\phi_1''}{3!} + \dots \right] - \frac{\phi_2'' \tau_{\text{in}}}{\phi_1''} \\
&+ \frac{\phi_2'' \Delta\Omega}{M} - \left[ \frac{\phi_2''}{\phi_f''} \left( \Omega_{\text{in}}^2 \frac{\phi_1''}{2!} + \Omega_{\text{in}}^3 \frac{\phi_1''}{3!} + \dots \right) \right] \\
&= M\tau_{\text{in}} + \left[ M \left( \Omega_{\text{in}}^2 \frac{\phi_1''}{2!} + \Omega_{\text{in}}^3 \frac{\phi_1''}{3!} + \dots \right) \right]. \quad (35)
\end{aligned}$$

Thus we see that the output time is given by the ideally magnified time plus a magnification of the temporal error introduced

while propagating through the input dispersion. Unlike output dispersive aberrations, input dispersive aberrations also distort the spectrum because of the temporal perturbation they introduce at the input to the lens.

### C. Dispersive Aberration Summary

Consider what these equations show about how dispersive aberrations affect the impulse response of a system. One might assume that if similar technologies are used for the input and output dispersive delay lines, the higher order spectral phase terms would be approximately related by the system magnification, i.e.,  $\phi_2''' \approx -M\phi_1'''$  since  $\phi_2'' = -M\phi_1''$  is required. Comparing (32) and (35), the difference in the temporal aberration produced is determined mainly by where the frequency of the ray is evaluated. A true impulse has an infinite bandwidth but the finite temporal aperture of the time lens would limit the transmitted signal to a finite bandwidth centered around  $\Omega = -\tau_{\text{in}}/\phi_1''$ , as shown by Ray #2 in Fig. 4, or slightly shifted in the case of input dispersive aberrations. For  $\Delta\Omega = 0$ , the input frequency  $\Omega_{\text{in}}$  in the input dispersive aberration case (35) is the same as the lens output frequency  $\Omega_{L,\text{out}}$  for the output dispersive aberration case (32), thus the temporal error introduced to the impulse response arrival time is approximately the same.

Blurring in the shape of the impulse response will be produced by variations in the temporal aberration over the bandwidth originating from a given input time. The  $\Delta\Omega/M$  term in (31) dramatically changes the transmitted bandwidth originating from  $\tau_{\text{in}}$ . For a system with large magnification,  $|M| \gg 1$ , the input dispersive aberrations will contribute much more substantially to distorting the impulse response shape than will contributions at the output because of the much broader bandwidth at the input. For a system with large compression,  $|M| \ll 1$ , these roles are exchanged because the larger bandwidth is then at the output.

It is also important to consider that signals of common interest in ultrafast optical systems may have bandwidths comparable to that of the time lens modulation and thus may be more appropriately viewed as the temporal analog to spatial beams propagating through lens systems. A signal made up of a series of pulses at the carrier frequency  $\omega_0$ , equivalent to all being centered at  $\Omega_{\text{in}} = 0$ , would propagate with a constant temporal offset through the input GDD, analogous to beams propagating parallel to the optical axis in space. In this case, input aberrations would not significantly affect the arrival time, only the shape of the signal as discussed above. For a system with large magnification, the output dispersion would be expected to primarily distort the output time of the pulse in accordance with (32), where the central output frequency for each pulse is  $\Omega_{L,\text{out}} \approx -\tau_{\text{in}}/\phi_f''$ . The output time versus input time is now

$$\tau_{\text{out}} = M\tau_{\text{in}} + \left[ \left( \frac{\tau_{\text{in}}}{\phi_f''} \right)^2 \frac{\phi_f'''}{2!} - \left( \frac{\tau_{\text{in}}}{\phi_f''} \right)^3 \frac{\phi_f''''}{3!} + \dots \right] \quad (36)$$

where  $M$  is the ideal linear magnification without this aberration. The observed magnification  $\tau_{\text{out}}/\tau_{\text{in}}$  is now curved by the output dispersive aberrations.

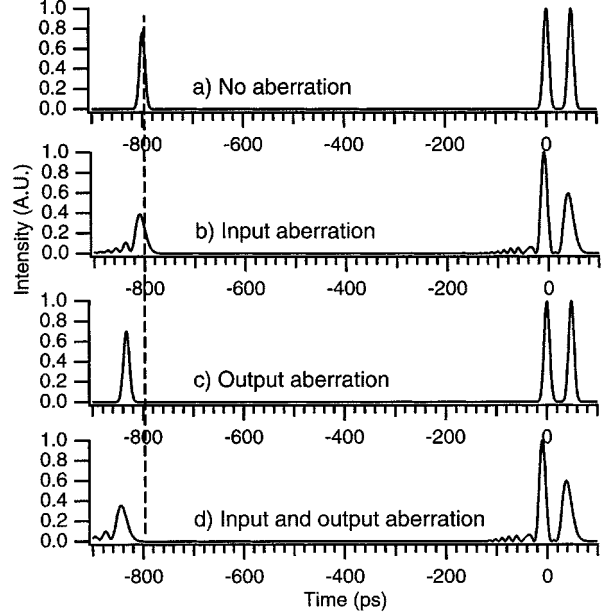


Fig. 6. Modeled temporal images of a three-pulse input waveform from a system with  $M = +100$ . The figure shows the effect of input and output dispersive aberrations  $\phi_1'''$  and  $\phi_2'''$ .

These effects are shown in the full envelope modeling results of Fig. 6. This model is for a DFG temporal imaging system with magnification of  $M = +100$ , a time lens pump of 20-ps FWHM, and linear chirp producing a focal dispersion  $\phi_f'' = -(d\omega/d\tau)^{-1} = (2\pi \times 275.8 \text{ GHz/ps})^{-1}$ . The input test pattern is three 100-fs FWHM Gaussian pulses at  $\tau_{\text{in}} = 0.5, 0.0$ , and  $-8.0$  ps. The aberration included is that due to  $\phi'''$  with the ratio  $\beta'''/\beta''$  equal to that of fused silica at  $\lambda = 1.55 \mu\text{m}$ . Clearly, including input dispersive aberrations in Fig. 6(b) dramatically changes the shape of the pulses while only a slight shift in the pulse timing is observed. With only the output dispersive aberrations in Fig. 6(c), we see that the shapes of the pulses are still very Gaussian but that the pulse out at the edge of the field of view has been shifted an extra 4% from its ideal location. Including both input and output dispersive aberrations in Fig. 6(d) produces an accumulated effect. Fortunately the dominant effect of an aberration helps identify its source and thus can be used to improve the system.

### D. Time Lens Aberrations

Now let us consider ideal input and output dispersive delay lines with aberration introduced by a higher order time lens phase modulation. Given a time ray with an input time  $\tau_{\text{in}}$  and a frequency  $\Omega_{\text{in}} = (-\tau_{\text{in}}/\phi_1'') + \Delta\Omega$ , the time and frequency at the input to the time lens are  $\tau_{L,\text{in}} = \phi_1''\Delta\Omega$  and  $\Omega_{L,\text{in}} = \Omega_{\text{in}}$ . The time out of the lens is unchanged,  $\tau_{L,\text{out}} = \tau_{L,\text{in}}$ , but it is frequency shifted to

$$\begin{aligned} \Omega_{L,\text{out}} &= \Omega_{L,\text{in}} + \tau_{L,\text{in}}\Phi'' + \left[ \tau_{L,\text{in}}^2 \frac{\Phi'''}{2!} + \tau_{L,\text{in}}^3 \frac{\Phi''''}{3!} + \dots \right] \\ &= \frac{-\tau_{\text{in}}}{\phi_1''} + \frac{\Delta\Omega}{M} + \left[ \tau_{L,\text{in}}^2 \frac{\Phi'''}{2!} + \tau_{L,\text{in}}^3 \frac{\Phi''''}{3!} + \dots \right] \end{aligned} \quad (37)$$

where  $\phi_f'' = -1/\Phi''$  is used in (21) to simplify the above expression. The output frequency is the same as produced by the lens,  $\Omega_{\text{out}} = \Omega_{L,\text{out}}$ , but after the output dispersion the time is

$$\tau_{\text{out}} = M\tau_{\text{in}} + \left[ \phi_2'' \left( \tau_{L,\text{in}}^2 \frac{\Phi'''}{2!} + \tau_{L,\text{in}}^3 \frac{\Phi''''}{3!} + \dots \right) \right]. \quad (38)$$

We see that there is both a spectral and temporal perturbation that depends on the arrival time of the ray at the lens and the nonlinearity of the time lens chirp.

In an idealized case, the infinite bandwidth of an impulse input would disperse to overfill the lens. Assuming the time lens phase aberrations are at least small over the duration of its transmission function  $P(\tau)$ , the majority of the transmitted signal would have propagated through the lens close enough to  $\tau_{L,\text{in}} \approx 0$  as to not be perturbed significantly; thus, there is very little distortion of the impulse response arrival time. Rays propagating through the outer edges of the time lens are perturbed, producing a distortion to the shape of the response. Odd-order temporal phase terms will produce a blurring to one side of the image, similar to the blur produced by coma in spatial systems. Even order terms produce a blurring that is symmetric and more analogous to spherical aberrations in spatial systems.

The light from a short temporal feature with a finite bandwidth may propagate through the time lens near one edge, similar to how a beam could propagate in space. In this case, both the output time and center frequency would be distorted approximately as given by (37) and (38) for the pulse's central time ray (spectral component). The time lens pupil function  $P(\tau)$  and spectral filtering effects [23] can shift the center of the transmitted spectrum slightly, modifying the total effect on a pulse from that predicted by calculations of a single ray.

Fig. 7 shows several temporal rays propagating from an ultrashort input pulse, through a system containing a lens with a third-order temporal phase, and forming a distorted output temporal image. The system is configured for  $-3\times$  magnification and uses the same time lens as in Fig. 3. The lens has again been shaded to visualize  $P(\tau)$  and the thickness of rays has been changed to indicate relative magnitudes of each spectral component. The output waveform was calculated using the envelope modeling expressions in Table I and shows a distortion to one side consistent with the ray diagram.

### E. Total System Aberrations

To first order in the resulting perturbation, the total ray aberration of a system with multiple sources is simply the summation of the individual results. Thus, a summation of the terms in square brackets from (32), (35), and (38) approximately gives the total temporal aberration of a particular ray. The best overall system performance will be achieved by designing each component to have no aberrations, but if one aberration source is unavoidable, introducing others to minimize this summation over the spectral and temporal range of interest can perform system-wide aberration minimization for a given application.

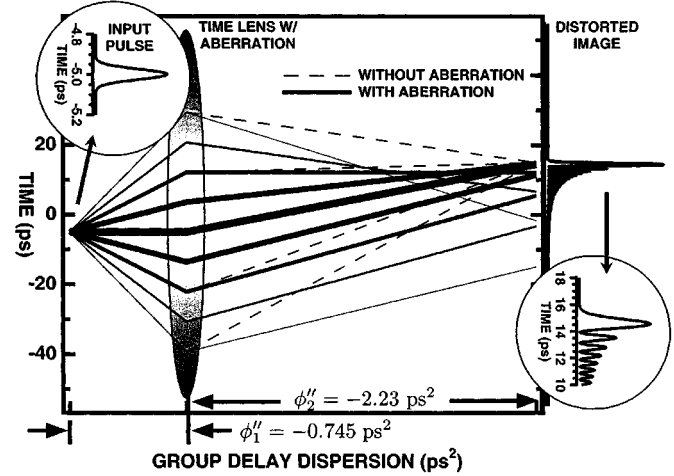


Fig. 7. A calculated ray diagram of an imaging system with  $M = -3$  and aberration produced by a third-order time lens phase. The effect is similar to coma in spatial imaging systems. The input is a transform-limited 60-fs pulse. The input rays span from  $-2\Omega_{\text{HM}}$  (top) to  $2\Omega_{\text{HM}}$  (bottom).

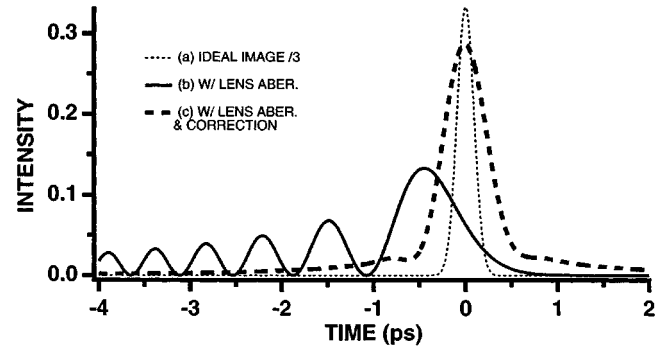


Fig. 8. System aberration minimization by combining different aberration sources. The imaging system is the same as in Fig. 7 with the input pulse at  $\tau_{\text{in}} = 0$ . The calculated output waveforms are with: (a) an ideal lens and no other aberration sources; (b) the same third-order time lens phase  $\Phi'''$  as in Fig. 7; and (c) time lens aberration corrected by adding input dispersive aberration  $\phi_1'''$  ( $\phi_2''' = 0$ ), in accordance with (40), to minimize the cumulative on-axis effect.

For example, consider a system with all three sources of third-order phase, resulting in the aberrated output time

$$\tau_{\text{out}} \approx M\tau_{\text{in}} + \left[ M \left( \frac{-\tau_{\text{in}}}{\phi_1''} + \Delta\Omega \right)^2 \frac{\phi_1'''}{2!} + \left( \frac{-\tau_{\text{in}}}{\phi_1''} + \frac{\Delta\Omega}{M} \right)^2 \frac{\phi_2'''}{2!} + \phi_2'' (\phi_1'' \Delta\Omega)^2 \frac{\Phi'''}{2!} \right]. \quad (39)$$

In an application where the on axis ( $\tau_{\text{in}} \approx 0$ ) impulse response shape is of primary importance, balancing the third-order phase such that

$$M\phi_1''' + \phi_2'''/M^2 + \phi_1''^2 \phi_2'' \Phi''' = 0 \quad (40)$$

would remove the temporal ray aberration at the output for all input frequencies and improve the impulse response shape. This can be seen in Fig. 8, where input dispersive aberration was added ( $\phi_1''' = -7.1723 \times 10^{-3} \text{ ps}^3$ ,  $\phi_2''' = 0$ ) in accordance with (40) to improve the on axis response of the system in Fig. 7.

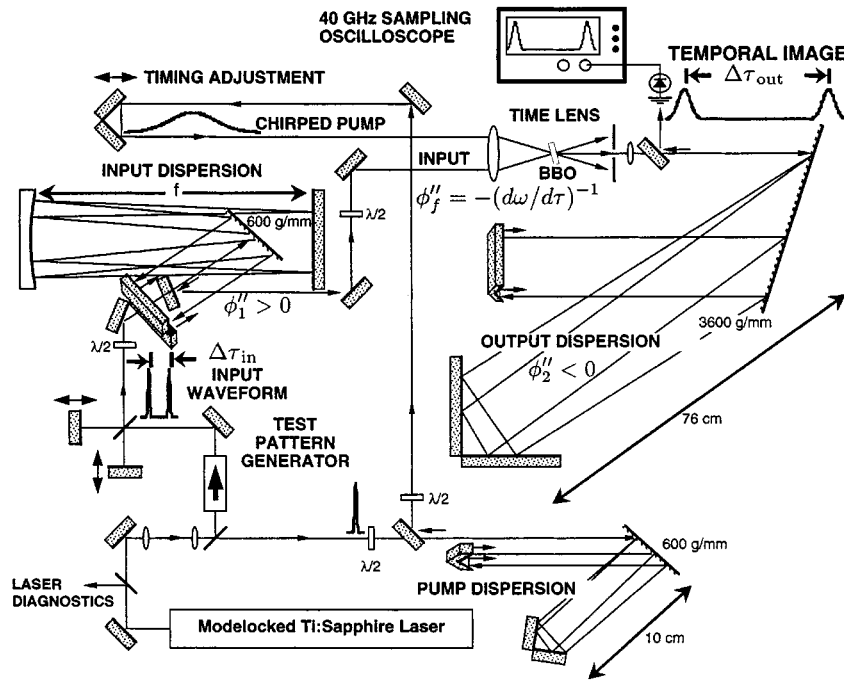


Fig. 9. Temporal imaging system configuration [31]. The dispersive delay lines are constructed with folded and multipassed grating systems. The time lens is produced by sum-frequency generation with a chirped optical pump pulse.

Adding the dispersive aberration has removed the series of pre-pulses generated by the time lens aberration, instead producing a single shorter pulse and a broad pedestal.

## VI. EXPERIMENTAL RESULTS

The configuration (Fig. 9) and experimental results of a parametric temporal imaging system with  $103\times$  temporal magnification and better than 178 fs resolution (including final recording system) have been reported [19], [20]. Recently, more detailed measurements of this system were performed over a longer temporal range and revealed further details of aberrations and misfocus.

The experiment used a modelocked Ti:Sapphire laser, producing time-bandwidth limited 87-fs ( $\Delta\omega = 30 \times 10^{12}$  rad/s) pulses at a center wavelength of 830 nm as the source from which both the input test pattern and time lens pump pulse were generated. Since the input and pump were at the same wavelength, an SFG time lens resulted in an output wavelength of 415 nm. Because of the peak power handling requirements of the input and pump dispersive delay lines, the difficulty in producing guided wave structures at a 415-nm wavelength, and the need for adjustability, we used diffraction grating delay lines [18] and [41].

The system was initially designed for a magnification of  $M = +100$  and a temporal field of view [23], or record length, of approximately 5-ps FWHM. The pump GDD, the physical GDD used to create the chirped pump, was set approximately and then measured using Spectrally Resolved Up-conversion [40] (see Fig. 10). Since the input pulse was initially time-bandwidth limited, the focal GDD is opposite that used to create the chirped pump  $\phi_f'' = -\phi_p''$ . Once the pump GDD was set, the required input and output GDDs were calculated using the

measured focal GDD and the desired magnification. The input dispersion was repeatedly adjusted and measured (Fig. 11) until it was 1% less than the focal dispersion, as required by (21) for  $M = +100$ . The output dispersion was then set for its desired value using the measured angles and grating spacing but the actual GDD was not measured. The measurements reported here were taken at a later date, with the changes indicative of system stability and measurement errors.

The chirped pump was generated by splitting off 50% of the laser beam and dispersing it in a folded and multipassed grating dispersive delay line [18]. The grating had 600 lines/mm and was set at an incident angle of  $25.0^\circ$ . While designing the system, it was observed that the third-order phase  $\phi_p'''$  imparted by a commercially available dielectric mirror was opposite in sign and one-quarter the magnitude of the expected third-order for the planned grating system. Its GDD was only 1% of that desired; thus, these mirrors could be added to the grating system and easily compensated for by adjusting the grating spacing. They were used for the horizontal folding mirrors, which reflect the beam a total of four times, thereby removing the expected third-order term from the pump dispersion system. Without this aberration correction, the third-order aberration strength (12), evaluated at the half maximum frequency  $\Omega_{HM} = \Delta\omega/2$ , was expected to be around  $(\Omega_{HM}\phi_p''')/(2!\phi_p'') \approx -0.01$ . Although already small, an order of magnitude reduction was expected by adding these mirrors. The measured pump dispersion (Fig. 10) shows no sign of higher order dispersion, with the fit giving  $\phi_p'' = -0.17666 \text{ ps}^2 \pm 0.00049 \text{ ps}^2$  (or  $\pm 0.28\%$ ).

The other 50% of the laser beam passed through an optical isolator and Michelson interferometer used to generate a two pulse test pattern. The delay arms of the Michelson were adjusted with  $\pm 0.67$ -fs round trip resolution. The signal then propagated through a positive dispersive delay line. It used

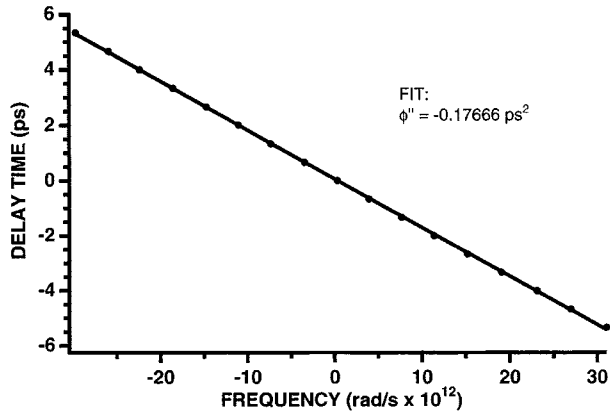


Fig. 10. Spectrally Resolved Up-conversion [37] measurement of the pump dispersion. Third-order phase of the grating system was canceled by that of four dielectric mirror reflections. Focal dispersion is opposite that of this physical pump dispersion  $\phi_f'' = -\phi_p''$ .

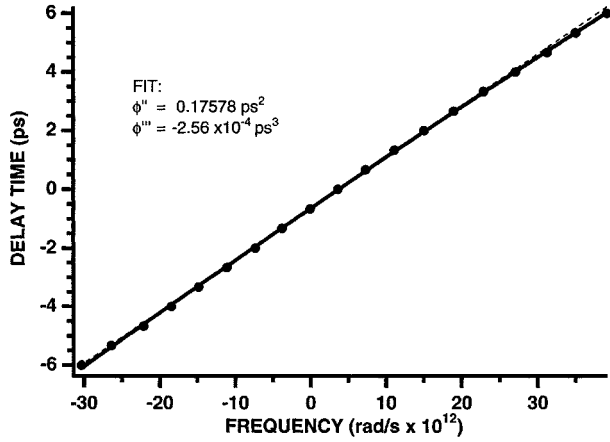


Fig. 11. Spectrally Resolved Up-conversion [40] measurement of the input dispersion.

a 600 lines/mm grating set at an incident angle of  $23.17^\circ$ . The system was folded vertically and made to have positive GDD using an off-axis telescope which consisted of a parabolic mirror and flat mirror one focal length away [41]. A pair of metallic mirrors, normal to each other, were also used to displace the beam vertically and send it on a second pass through the system. The GDD of the optical isolator, Michelson components, and grating system were treated as one total input GDD system and measured together (Fig. 11), resulting in  $\phi_1'' = 0.17578 \text{ ps}^2 \pm 0.0006 \text{ ps}^2$  (or  $\pm 0.34\%$ ) and  $\phi_1''' = -2.56 \times 10^{-4} \text{ ps}^3 \pm 5.6 \times 10^{-5} \text{ ps}^3$ . The relative strength of third-order aberration (12) is  $(\Omega_{\text{HM}} \phi_1''') / (2! \phi_1'') = -0.012$ . Although very small, it is apparent in Fig. 11 only because the measurement was made over a spectral range wider than the full width at half maximum.

The temporal phase of the pump pulse was imparted to the signal by mixing them in a  $500 \mu\text{m}$  thick beta-barium borate (BBO) crystal. The crystal was cut at  $28.1^\circ$  and used in a non-collinear type-I phase-matching configuration. Although angle tuned to phase-match the carrier frequencies, the 94 fs group delay difference between the fundamental and upconverted signals propagating through the crystal produced a slight filtering effect at the output of the system. This effect is insignificant to

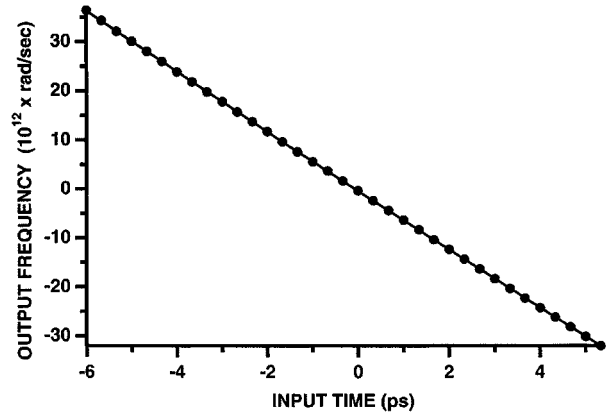


Fig. 12. Frequency out (relative to a carrier at  $\lambda = 415 \text{ nm}$ ) versus input time for one pulse.  $d\Omega_{\text{out}}/d\tau_{\text{in}} = -6.0244 \times 10^{12} \text{ rad/s/ps}$ .

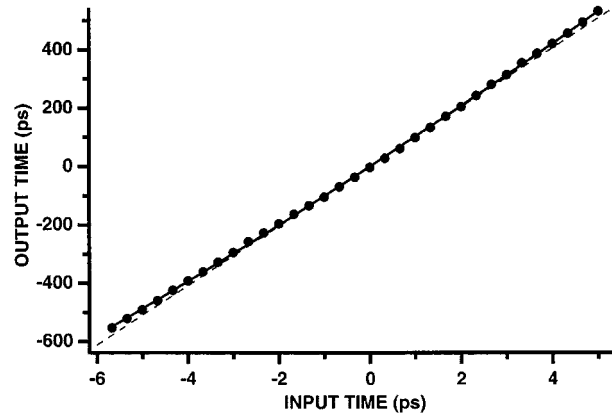


Fig. 13. Output time versus input time for one pulse, centered at  $\Omega_{\text{in}} = 0$ , scanned through the field of view. Fit gives  $\tau_{\text{out}} = 102.0\tau_{\text{in}} + (0.905/\text{ps})\tau_{\text{in}}^2$ .

the system impulse response width but does slightly reduce the temporal field of view [23].

The output dispersive delay line was constructed with a similar folded and multipassed design as the pump dispersion. The output signal, now at a center wavelength of  $\lambda = 415 \text{ nm}$ , was dispersed by a 3600 lines/mm grating. The angle of incidence was  $42.8^\circ \pm 0.1^\circ$ . Although the folding mirrors were dielectric, their single stack design had a dispersion insignificant in comparison to that of the grating system and were, therefore, ignored. The grating-to-grating path length along the beam is  $171.5 \text{ cm} \pm 1.0 \text{ cm}$  (or  $\pm 0.6\%$ ). The calculated output dispersion parameters are  $\phi_2'' = -16.719 \text{ ps}^2$  and  $\phi_2''' = 0.05102 \text{ ps}^3$ , producing an aberration strength at the half maximum frequency of  $(\Omega_{\text{HM}} \phi_2''') / (2! \phi_2'') = -0.024$ .

The most significant aberration expected in this system was that due to the output third-order spectral phase  $\phi_2'''$ . While not affecting the output spectrum or significantly changing the pulse width, its presence in the system would produce a curved output time versus input time. To test for this aberration, the output spectrum and temporal image of a single input pulse (centered at  $\lambda = 830 \text{ nm}$  or  $\Omega_{\text{in}} = 0$ ) were recorded for numerous input times  $\tau_{\text{in}}$  and their peak locations plotted in Figs. 12 and 13.

The measured width of the output spectrum was always 0.1 nm, limited by the resolution of the spectrometer and optical multichannel analyzer, but its central wavelength (frequency in

the figure) varied linearly with the input time (Fig. 12), consistent with our prediction of insignificantly small time lens aberrations. Ignoring aperture effects, the expected output center frequency is  $\Omega_{\text{out}} = -\tau_{\text{in}}/\phi_f'' = \tau_{\text{in}} \times (-5.6606) \times 10^{12}$  rad/s/ps. The measured slope of  $d\Omega_{\text{out}}/d\tau_{\text{in}} = -6.0244 \times 10^{12}$  rad/s/ps is 6% more negative. This is because our measurements are actually of the peak spectral locations for a superposition of rays (spectral components) under conditions where an apodization produced by  $P(\tau)$  causes preferential transmission of rays passing through the center of the lens and thus shifts the peak of the spectrum.

The recorded temporal images had a width of 24 ps and varied in output time as shown in Fig. 13. This linear magnification of  $M = +102$  is 1% less than reported earlier [19], [20]. Measuring the output signal over a longer range of input times has resolved a curvature in the magnified pulse timing. Using the pulse's central time ray at  $\Omega_{\text{in}} = 0$  (or equivalently  $\Delta\Omega = \tau_{\text{in}}/\phi_f''$ ) to predict the signal timing, the expected output time versus input time is

$$\tau_{\text{out}} = \left(1 - \frac{\phi_2''}{\phi_f''}\right) \tau_{\text{in}} + \frac{\phi_2'''}{2!} \left(\frac{\tau_{\text{in}}}{\phi_f''}\right)^2 \quad (41)$$

including the possibility of a slight misfocus and the third-order output aberration in (36). Fitting the measured data in Fig. 13 to (41), using the measured focal GDD  $\phi_f'' = 0.17666$  ps<sup>2</sup> found in Fig. 10 gives  $\phi_2'' = -17.843$  ps<sup>2</sup> and  $\phi_2''' = 0.0565$  ps<sup>3</sup>. These values are 6.7% and 10.7% greater in magnitude than expected, respectively. The reason is the spectral pulling effect mentioned above. Calculating a fit to the data in Fig. 13 using the measured  $d\Omega_{\text{out}}/d\tau_{\text{in}}$  from Fig. 12 in place of  $-1/\phi_f''$  in (41) gives  $\phi_2'' = -16.765$  ps<sup>2</sup> and  $\phi_2''' = 0.04987$  ps<sup>3</sup>, 0.3% greater and 2.3% less in magnitude than expected, respectively. The observed curvature in the magnified output time is, thus, consistent with the expected output dispersive aberration.

The average width of the output pulses reported in [19], [20] was 18.3-ps FWHM. Deconvolving the 12.5-ps FWHM impulse response of the recording electronics and the  $103 \times 87$  fs = 8.96-ps FWHM width of an ideally magnified pulse results in a temporal imaging system impulse response width of approximately 9.89 ps, or 96 fs referred to the input. This system's ideal impulse response width is also 8.96 ps, or 87 fs referred to the input, determined by its initially transform-limited Gaussian pump pulse duration [23]. The observed 10.3% blurring is actually very good considering that the uncertainty in the measurements of  $\phi_f''$  and  $\phi_f'''$  were each approximately  $\pm 0.3\%$  and the lens aperture was 5.7-ps FWHM. From the discussion at the end of Section IV.C, we might have expected blurring as high as 60% of the aperture width, or about 38% of the ideal response width, simply because of the uncertainty in the focus.

Although not intentionally changed, the pump and input GDD measurements (Figs. 10 and 11) are, respectively, 0.16% and 0.66% less than what was reported earlier [19], [20]. This indicates a possible 50% error in the bandwidth reduction factor in (28), which produces a misfocus in (29). A third set of measurements taken much later resulted in GDD increases of 0.03% and 0.42%. These changes are most likely due to the uncertainty of

the measurement technique (at least  $\pm 0.3\%$  from fits) and the stability of the pump laser. A spectrometer with a 0.3-nm resolution monitored the laser and the center wavelength was observed drifting slightly during the day. Theoretically, an uncertainty in the center wavelength of  $\pm 0.6$  nm produces an uncertainty in the pump and input dispersions of  $\pm 0.22\%$ . Although these errors are very small, they produce a significant blurring effect. Deconvolving the impulse response of the recording electronics and the ideal temporal imaging width from the measured 24-ps signal pulses obtained here gives an imaging system impulse response of 18.5-ps FWHM, approximately double the ideal value. Clearly small changes caused the system to drift out of focus. Blurring due to higher order phase aberrations in this system are insignificant in comparison to the focus uncertainty.

## VII. CONCLUSION

Ideal temporal imaging components must impart a quadratic phase, either spectrally for the dispersive delay lines, or temporally for the time lens modulation. The departure of any realistic component's phase from this idealized form will introduce aberrations in the system, the results of which vary depending on the system configuration, the type of aberration, and its location in the system. Aberrations were studied theoretically using both full envelope modeling and the propagation of "time rays." We have shown that the ray approach is a simple way to describe the space-time flow of energy in these systems and a useful tool for investigating the results of aberrations. Aberrations were measured in an experimental system and found to agree well with theory. Like its spatial counterpart, the study of aberrations in temporal imaging systems is a rich field, critical to development of real instrumentation. The work presented here should serve as a foundation on which further analysis is performed.

Constructing an imaging system with ultrafast resolution and large magnification ( $|M| \gg 1$ ) or compression ( $|M| \ll 1$ ) requires an active modulation process configured such that the magnitude of its focal dispersion is a very small and precise difference from that of either the input or output dispersion. We have found that setting and maintaining the proper focus is a challenging task. It requires highly precise measurement techniques and very stable components.

## REFERENCES

- [1] J.-C. Diels and W. Rudolph, *Ultrashort Laser Pulse Phenomena*. New York: Academic, 1996.
- [2] M. W. Kimmel, R. Trebino, J. K. Ranka, R. S. Windeler, and A. J. Stentz, "Measuring the intensity and phase of ultrabroadband continuum," in *Proc. CLEO 2000*, San Francisco, CA, May 2000, Paper CFL7.
- [3] R. Trebino, K. W. DeLong, D. N. Fittinghoff, J. N. Sweetser, M. A. Krumbügel, and D. J. Kane, "Measuring ultrashort laser pulses in the time-frequency domain using frequency-resolved optical gating," *Rev. Sci. Instrum.*, vol. 68, pp. 3277–3295, 1997.
- [4] A. Baltuška, M. S. Pshenichnikov, and D. A. Wiersma, "Second-harmonic generation frequency-resolved optical gating in the single-cycle regime," *IEEE J. Quantum Electron.*, vol. 35, pp. 459–478, 1999.
- [5] P. Tournois, J.-L. Verner, and G. Bienvenu, "Sur l'analogie optique de certains montages électroniques: Formation d'images temporelles de signaux électriques," *C. R. Acad. Sci.*, vol. 267, pp. 375–378, 1968.
- [6] W. J. Caputi, "Stretch: A time transformation technique," *IEEE Trans. Aerosp. Electron. Syst.*, vol. AES-7, pp. 269–278, 1971.
- [7] L. S. Telegin and A. S. Chirkin, "Reversal and reconstruction of the profile of ultrashort light pulses," *Sov. J. Quantum Electron.*, vol. 15, pp. 101–102, 1985.

- [8] S. A. Akhmanov, V. A. Vysloukh, and A. S. Chirkin, "Self-action of wave packets in a nonlinear medium and femtosecond laser pulse generation," *Sov. Phys. Usp.*, vol. 29, pp. 642–677, 1987.
- [9] B. H. Kolner and M. Nazarathy, "Temporal imaging with a time lens," *Opt. Lett.*, vol. 14, pp. 630–632, 1989, and erratum vol. 15, p. 655, 1990.
- [10] B. H. Kolner, "Space-time duality and the theory of temporal imaging," *IEEE J. Quantum Electron.*, vol. 30, pp. 1951–1963, Aug. 1994.
- [11] —, "Generalization of the concepts of focal length and  $f$ -number to space and time," *J. Opt. Soc. Am. A*, vol. 11, no. 12, pp. 3229–3234, Dec. 1994.
- [12] P. Naulleau and E. Leith, "Stretch, time lenses, and incoherent time imaging," *Appl. Opt.*, vol. 34, no. 20, pp. 4119–4128, 1995.
- [13] C. V. Bennett and B. H. Kolner, "Subpicosecond single-shot waveform measurement using temporal imaging," presented at the Proc. LEOS'99 Conference, Paper ThBB1, 1999.
- [14] P. Tournois, "Analogie optique de la compression d'impulsion," *C. R. Acad. Sci.*, vol. 258, pp. 3839–3842, Apr. 1964.
- [15] A. Papoulis, *Systems and Transforms with Applications in Optics*. New York: McGraw-Hill, 1968.
- [16] S. A. Akhmanov, A. S. Chirkin, K. N. Drabovich, A. I. Kovrigin, R. V. Khokhlov, and A. P. Sukhorukov, "Nonstationary nonlinear optical effects and ultrashort light pulse formation," *IEEE J. Quantum Electron.*, vol. QE-4, pp. 598–605, 1968.
- [17] S. A. Akhmanov, A. P. Sukhorukov, and A. S. Chirkin, "Nonstationary phenomena and space-time analogy in nonlinear optics," *Sov. Phys.—JETP*, vol. 28, pp. 748–757, 1969.
- [18] E. B. Treacy, "Optical pulse compression with diffraction gratings," *IEEE J. Quantum Electron.*, vol. QE-5, pp. 454–458, 1969.
- [19] C. V. Bennett and B. H. Kolner, "Upconversion time microscope demonstrating  $103\times$  magnification of femtosecond waveforms," *Opt. Lett.*, vol. 24, no. 11, pp. 783–785, June 1999.
- [20] —, "Parametric temporal imaging," in *Ultrafast Electronics and Optoelectronics*, J. Bowers and W. Knox, Eds. Washington, DC: Opt. Soc. Amer., Aug. 1999, pp. 53–62. vol. 28 of *Trends in Optics and Photonics Series*.
- [21] C. V. Bennett and B. H. Kolner, "Principles of parametric temporal imaging—Part I: System configurations," *IEEE J. Quantum Electron.*, vol. 36, pp. 430–437, Apr. 2000.
- [22] S. P. Dijailli, A. Dienes, and J. S. Smith, "ABCD matrices for dispersive pulse propagation," *IEEE J. Quantum Electron.*, vol. 26, pp. 1158–1164, June 1990.
- [23] C. V. Bennett and B. H. Kolner, "Principles of parametric temporal imaging—Part II: System performance," *IEEE J. Quantum Electron.*, vol. 36, pp. 649–655, June 2000.
- [24] D. Marcuse, "Pulse distortion in single-mode fibers," *Appl. Opt.*, vol. 19, pp. 1653–1660, 1980.
- [25] J. A. Giordmaine, M. A. Duguay, and J. W. Hansen, "Compression of optical pulses," *IEEE J. Quantum Electron.*, vol. QE-4, pp. 252–255, 1968.
- [26] D. R. Grischowsky, "Optical pulse compression," *Appl. Phys. Lett.*, vol. 26, pp. 566–568, 1974.
- [27] J. E. Bjorkholm, E. H. Turner, and D. B. Pearson, "Conversion of cw light into a train of subnanosecond pulses using frequency modulation and the dispersion of a near-resonant atomic vapor," *Appl. Phys. Lett.*, vol. 26, pp. 564–566, 1975.
- [28] J. K. Wigmore and D. R. Grischowsky, "Temporal compression of light," *IEEE J. Quantum Electron.*, vol. QE-14, pp. 310–315, 1978.
- [29] B. H. Kolner, "Active pulse compression using an integrated electro-optic phase modulator," *Appl. Phys. Lett.*, vol. 52, no. 14, pp. 1122–1124, 1988.
- [30] A. A. Godil, B. A. Auld, and D. M. Bloom, "Picosecond time-lenses," *IEEE J. Quantum Electron.*, vol. 30, pp. 827–837, Mar. 1994.
- [31] B. H. Kolner, C. V. Bennett, and R. P. Scott, "Space-time duality and temporal imaging," *Proc. SPIE OE/LASE*, vol. 2116, 1994.
- [32] M. T. Kauffman, A. A. Godil, W. C. Banyai, and D. M. Bloom, "Applications of time lens optical systems," *Electron. Lett.*, vol. 29, pp. 268–269, 1993.
- [33] G. P. Agrawal, P. L. Baldeck, and R. R. Alfano, "Temporal and spectral effects of cross-phase modulation on copropagating ultrashort pulses in optical fibers," *Phys. Rev. A*, vol. 40, pp. 5063–5072, 1989.
- [34] C. V. Bennett, R. P. Scott, and B. H. Kolner, "Temporal magnification and reversal of 100 Gb/s optical data with an up-conversion time microscope," *Appl. Phys. Lett.*, vol. 65, no. 20, pp. 2513–2515, Nov. 1994.
- [35] J. P. Heritage, A. M. Weiner, and R. N. Thurston, "Picosecond pulse shaping by spectral phase and amplitude manipulation," *Opt. Lett.*, vol. 10, pp. 609–611, 1985.
- [36] A. M. Weiner, J. P. Heritage, and E. M. Kirschner, "High resolution femtosecond pulse shaping," *J. Opt. Soc. Am. B*, vol. 5, pp. 1563–1572, 1988.
- [37] A. E. Conrady, *Applied Optics and Optical Design*. New York: Dover, 1957, 1960, vol. 1 and 2.
- [38] W. J. Smith, *Modern Optical Engineering*. New York: McGraw-Hill, 1966.
- [39] F. A. Jenkins and H. E. White, *Fundamentals of Optics*, 4th ed. New York, NY: McGraw-Hill, 1976.
- [40] J.-P. Foing, J.-P. Likforman, M. Joffre, and A. Migus, "Femtosecond pulse phase measurement by spectrally resolved up-conversion: Application to continuum compression," *IEEE J. Quantum Electron.*, vol. 28, pp. 2285–2290, Oct. 1992.
- [41] O. E. Martinez, "3000 times grating compressor with positive group velocity dispersion: Application to fiber compression in the 1.3–1.6  $\mu\text{m}$  region," *IEEE J. Quantum Electron.*, vol. QE-23, pp. 59–64, 1987.



**Corey V. Bennett** (S'95) received the B.S. degree (*summa cum laude*) in laser electrooptics technology from Oregon Institute of Technology, Klamath Falls, in 1991 and the M.S. degree in electrical engineering from the University of California, Los Angeles (UCLA), in 1995. He is currently working toward the Ph.D. degree, majoring in electrical engineering at UCLA.

In 1991, he joined Prof. Kolner's Laser and Electro-optic Research Group at UCLA, which moved to the University of California, Davis, and a facility at Lawrence Livermore National Laboratory (LLNL), Livermore, CA, in 1996. He joined the Electronics Engineering Division at LLNL in 1998, where he continues his temporal imaging research through a collaboration with the Kolner Group and the LLNL Photonics Group.



**Brian H. Kolner** (S'79-M'79) received the B.S. degree in electrical engineering in 1979 from the University of Wisconsin, Madison, and the M.S. and Ph.D. degrees from Stanford University, Stanford, CA, in electrical engineering in 1981 and 1985, respectively.

From 1985 to 1991, he was a member of the technical staff at Hewlett-Packard Laboratories, Palo Alto, CA, where he worked on high-speed electronic and optoelectronic devices and measurement techniques using ultrashort laser pulses. In 1991, he joined the Electrical Engineering Department at the University of California, Los Angeles (UCLA), and became Vice Chairman for undergraduate affairs in 1993. At UCLA, he taught courses in microwave measurements, Fourier optics, and quantum mechanics, and conducted research in space-time duality and temporal imaging. In 1996, he moved to the University of California, Davis, where he holds joint appointments in the Departments of Applied Science and Electrical and Computer Engineering, and Lawrence Livermore National Laboratory, Livermore, CA. He teaches laser physics, electromagnetic theory, and optics, and his current research interests are in temporal imaging, laser phase and amplitude noise, and precision clocks and oscillators.

Dr. Kolner was awarded a David and Lucile Packard Foundation Fellowship in 1991 and served as Guest Editor for the IEEE JOURNAL OF SPECIAL TOPICS IN QUANTUM ELECTRONICS in 1996. He is a member of the Optical Society of America and the American Institute of Physics.